Biomaterials 266 (2021) 120436

Contents lists available at ScienceDirect

Biomaterials

journal homepage: www.elsevier.com/locate/biomaterials

3D alveolar *in vitro* model based on epithelialized biomimetically curved culture membranes

D. Baptista [a], L. Moreira Teixeira [a,b], Z. Tahmasebi Birgani [a], S. van Riet [c], T. Pasman [d], A. Poot [d], D. Stamatialis [d], R.J. Rottier [e], P.S. Hiemstra [c], P. Habibović [a], C. van Blitterswijk [a], S. Giselbrecht [a,1], R. Truckenmüller [a,*,1]

[a] MERLN Institute for Technology-Inspired Regenerative Medicine, Maastricht University, Universiteitssingel 40, 6229 ER, Maastricht, the Netherlands
[b] Department of Developmental BioEngineering, Technical Medical Centre, University of Twente, Drienerlolaan 5, 7522 NB, Enschede, the Netherlands
[c] Department of Pulmonology, Leiden University Medical Center, Albinusdreef 2, 2333 ZA, Leiden, the Netherlands
[d] Department of Biomaterials Science and Technology, Technical Medical Centre, University of Twente, Drienerlolaan 5, 7522 NB, Enschede, the Netherlands
[e] Department of Pediatric Surgery/Cell Biology, Erasmus (University) Medical Center – Sophia Children's Hospital, Doctor Molewaterplein 40, 3015 GD, Rotterdam, the Netherlands

ARTICLE INFO

Keywords:
Curvature
Alveolar epithelial cells
Ion track-etched membranes
Microthermoforming
Biomimetics
In vitro models

ABSTRACT

There is increasing evidence that surface curvature at a near-cell-scale influences cell behaviour. Epithelial or endothelial cells lining small acinar or tubular body lumens, as those of the alveoli or blood vessels, experience such highly curved surfaces. In contrast, the most commonly used culture substrates for *in vitro* modelling of these human tissue barriers, ion track-etched membranes, offer only flat surfaces. Here, we propose a more realistic culture environment for alveolar cells based on biomimetically curved track-etched membranes, preserving the mainly spherical geometry of the cells' native microenvironment. The curved membranes were created by a combination of three-dimensional (3D) micro film (thermo)forming and ion track technology. We could successfully demonstrate the formation, the growth and a first characterization of confluent layers of lung epithelial cell lines and primary alveolar epithelial cells on membranes shaped into an array of hemispherical microwells. Besides their application in submerged culture, we could also demonstrate the compatibility of the bioinspired membranes for air-exposed culture. We observed a distinct cellular response to membrane curvature. Cells (or cell layers) on the curved membranes reveal significant differences compared to cells on flat membranes concerning membrane epithelialization, areal cell density of the formed epithelial layers, their cross-sectional morphology, and proliferation and apoptosis rates, and the same tight barrier function as on the flat membranes. The presented 3D membrane technology might pave the way for more predictive barrier *in vitro* models in future.

1. Introduction

Geometric form and biological function of living systems are inherently linked together at all length scales [1,2]. The diversity of these systems or organisms is expressed in a wealth of forms, but with a striking prevalence for round(ed) shapes or curved surfaces. There is increasing evidence that surface curvature with curvature radii in a near-cell-range influences cell behaviour [3,4]. Epithelial and endothelial cells lining small acinar or tubular body lumens, as those of the lung alveoli, kidney tubules or blood vessels, reside on and experience such strongly curved surfaces. In contrast, the majority of the proven standard cell or tissue culture plastics offers only flat culture surfaces. Consequently, these geometrically always very similar, quite simple culture environments are in this respect also largely unspecific for the tissue or organ under study, not appropriately reflecting its (micro) anatomy.

This limitation also holds for ion track-etched porous membranes [5], which are probably the most commonly used culture substrates and the gold standard and reference material for *in vitro* modelling of human tissue barriers such as the afore-mentioned ones. Consequently, there is

* Corresponding author.
E-mail address: r.truckenmuller@maastrichtuniversity.nl (R. Truckenmüller).
[1] These authors equally contributed to this paper.

https://doi.org/10.1016/j.biomaterials.2020.120436
Received 13 February 2020; Received in revised form 30 August 2020; Accepted 6 October 2020
Available online 10 October 2020

a large data basis in the form of corresponding published scientific studies available. To this end, the membranes are typically integrated into cell culture inserts in well plates or microfluidic organ-on-a-chip devices, where they separate a bottom from a top well or fluidic compartment. Generally, membranes in these applications allow the establishment of co-cultures and air-liquid interface (ALI) cultures across the porous substrates. Ion track membranes outperform most other membranes concerning a number of aspects. Their circular-cylindrical pores running straight from one side of the membrane to its other side fully contribute to mass transfer such as by diffusion. At the same time, these pores only to a minimum extent mechanically weaken the membrane, which means very thin membranes can still be handled. The pores also only minimally add undesirable surface topography to the membrane, which otherwise could hinder the formation of defect-free confluent cell monolayers. And the pores only to a minimum extent unfavourably interfere with and obstruct the light passed through the membrane during microscopic imaging, with corresponding positive consequences for the image quality. The pores have a narrow diameter distribution, can have very high aspect ratios (meaning that membranes with very small pores can still stay with a manageable thickness) and their size can be adjusted independently from their areal density. Therefore, when employing

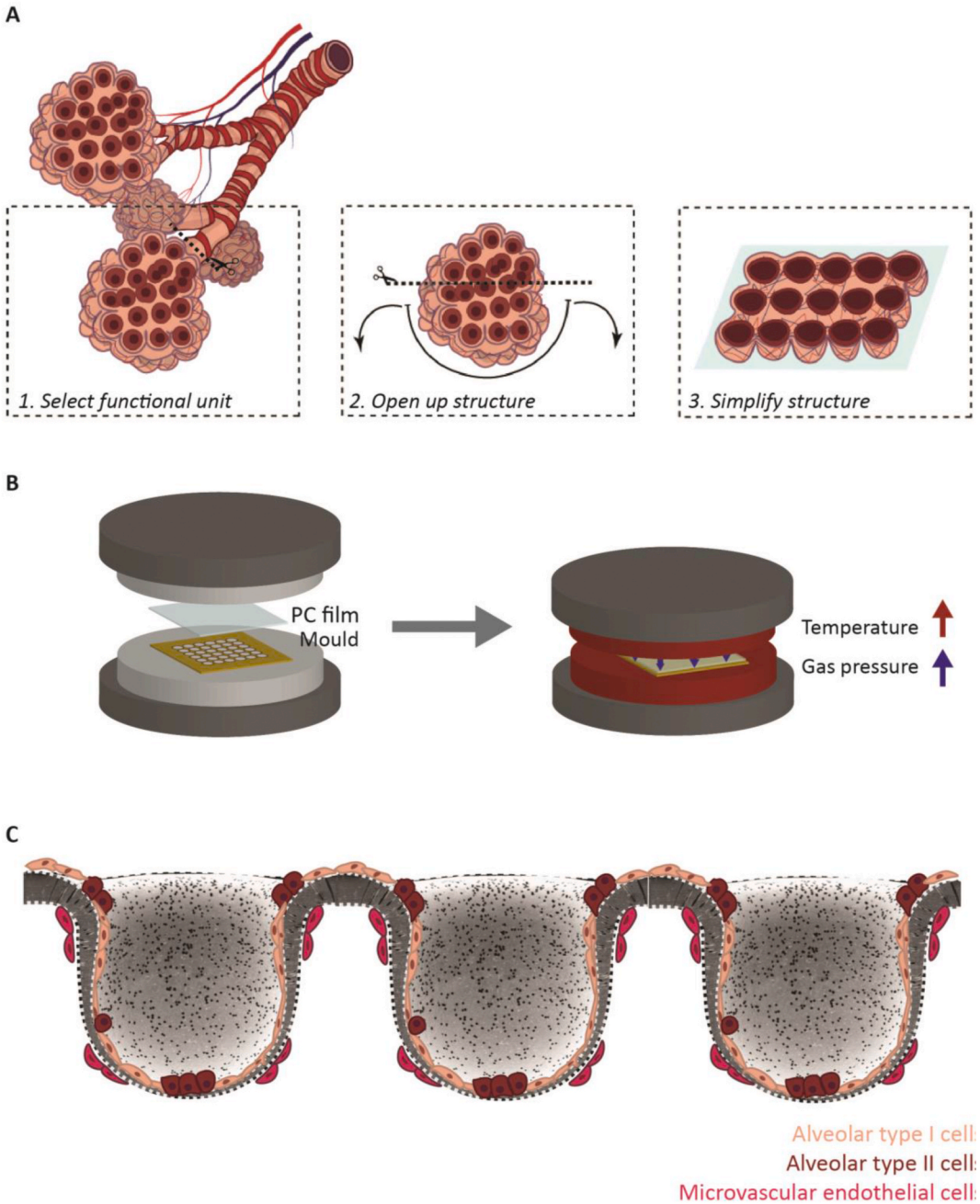

Fig. 1. Concept and microfabrication of biomimetically curved culture membranes. (A) Approach for the design of a bioinspired culture membrane for a 3D alveolar *in vitro* model: We conceptualized the alveolar sac as an open(ed) structure with the shape and size of the bioartificial alveoli being similar to that of the adult organ. **(B)** Curved culture membranes were created by gas-assisted microthermoforming of heavy ion-irradiated thin polymer films. By controlling forming temperature and (gas) pressure, it is possible to achieve uniform arrays of hemispherical microwells mimicking an 'open' alveolar sac. **(C)** After subsequent ion track etching, the resulting curved porous films/membranes allow the culture of alveolar epithelial cells on the concave inner side and, potentially, endothelial cells on the convex outer side, enabling the establishment of a model of the air-blood interface of the alveolar epithelial-endothelial/capillary barrier.

these membranes for *in vitro* models of barrier tissues, the diffusion of nutrients, gases, metabolites or signalling molecules, and a potentially desired or not desired cell migration are highly controllable. However, in view of the above-mentioned impact of curvature on cell behaviour, to more closely reflect *in vitro* the spatial cell arrangements related to tissue- or organ-specific curvature *in vivo*, the track-etched culture membranes would have to be correspondingly (micro)curved instead of just planar. This is the conceptual basis of the bioinspired three-dimensional (3D) lung alveolar *in vitro* model presented in this paper.

The primary function of our lungs is efficient oxygen and carbon dioxide exchange between the external milieu and the internal vascular space. This gas exchange is mainly accomplished by, in adult humans, around 80 m^2 total surface area [6] of the on average roughly 480 million pulmonary alveoli [7], taken both lungs together. In the last years, there has been much attention on delivering drugs via the pulmonary route, which is due to the large absorptive surface area of the lungs, the avoidance of the (hepatic) first-pass effect, and the possibility to deliver drugs locally to the lung in the case of pulmonary diseases [8]. This emphasizes the importance of corresponding *in vitro* research and test models. The particular relevance of alveolar *in vitro* models is also due to the fact that lung diseases affecting large numbers of patients, such as chronic obstructive pulmonary disease (COPD), are characterized by alveolar destruction [9]. Most of the existing knowledge on lung development, physiology, pathophysiology and pharmacokinetics stems from animal models [10]. Besides ethical issues of animal testing, these models often fail to reasonably recapitulate lung physiology of humans, highlighting the need for human *in vitro* models that help to complement existing models, while extending current understanding in the field.

Here, we propose a more realistic culture environment for lung alveolar cells based on biomimetically curved porous culture membranes, preserving or restoring the mainly spherical geometry of the cells' native microenvironment (Fig. 1A). The curved membranes were created by a technology pioneered by us that is based on microscale 3D film (thermo)forming [11] (Fig. 1B) of heavy ion-irradiated thin polymer films and subsequent ion track etching [12]. We investigated the forming and growing and conducted a first characterization of confluent layers of lung epithelial cell lines and commercially available primary alveolar epithelial cells on polycarbonate (PC) ion track membranes that were given the shape of an array of hemispherical microwells (Fig. 1C). We then compared the findings from the curved membranes with that of flat ones from the same material. Besides their usage in submerged culture, we also studied the compatibility of the bioinspired membranes with culture at the ALI.

2. Materials and methods

2.1. Rationale of design, fabrication and characterization of bioinspired culture membranes

Microcurved membranes were produced from 25 μm thin PC films (it4ip, Belgium), either (pre-)irradiated with 10^6 (heavy) ions/cm^2 to finally be track-etched and become porous, or non-irradiated to stay non-porous. Generally, ion-irradiated PC films already etched but also, as in our case, not yet etched are commercially available in thicknesses between approximately 5 and 50 μm. The membranes integrated into commercial culture inserts are typically around 10 μm thin. Square arrays of hemispherically shaped microwells with an inner diameter of approximately 200 μm, shape- and size-wise mimicking the anatomy of average human alveoli [7], were formed in the polymer films. This design represents of course only a limited approximation and certain simplification of the alveolar architecture, not taking into account the polyhedral geometry of the alveoli around the region of their (joined) septal walls [13]. The basic feasibility of such an approach was shown by us in an earlier study in conjunction with a different application [14]. There, arrays of similar-sized hemispherical wells that were hexagonally arranged and shaped at their upper rims were formed in 25 μm thin (dense) films from polylactic acid (PLA). The simpler, fully hemispherical design with consequently circular upper rims employed in this study was chosen to allow a more unobstructed view on the pure effect of curvature on the lung epithelial cells or cell layers when assessing the same in corresponding assays due to the fact that within the wells the curvature radius is everywhere the same. The film forming was conducted as a free-forming variant of the microthermoforming process as previously reported [11,12]. Non-porous irradiated and non-irradiated PC films were inflated and thereby stretched into 250-μm diameter cylindrical through-holes of a sheet-type brass mould each at a forming temperature and pressure of 153 °C and 11 bar, respectively. Between reaching the forming temperature, applying the forming pressure and cooling down, there were practically no dwell times. The wells are slightly deeper than the curvature radius of the wells because of the difference between the initial film thickness between the wells and the reduced film thickness in the wells, the latter due to thinning of the film in these regions as a result of (biaxial) film stretching. To always achieve the same/a very similar curvature radius also against slight variations of the forming depth, we aimed at forming the films even a little bit deeper (around additional 5 μm deeper). Due to the stretching of the film, but also always some erosion of the film surface(s) during the subsequent etching of the pores, the average wall thickness of the microwells is around 10 μm. It is therewith more or less the same as the thickness of the membranes in the commercial inserts. The microdrilled holes were arranged in a 9 × 9 array with 50-μm spacing between them. As also previously reported, the film forming occurs in a softened, but not flowing or melting state of the polymer. For this reason, during forming of the film, the latent ion tracks in the film are preserved for the subsequent (3D) track etching of pores after film forming [12,15]. The wet-chemical etching of the pores was performed by immersing the irradiated and formed films at 65 °C in a stirred aqueous solution of 5 mol/l NaOH and 10% (w/v) methanol. The pore size was controlled by adjusting the etching time, which was 15 min. The same process parameters as for the formed, curved irradiated films were applied to non-formed, flat irradiated films. The etching process was stopped by rinsing the etched film with deionized water and isopropanol. Prior to cell culture, the membranes were wetted and sterilized with an ethanol-water series at decreasing concentrations of ethanol, and washed with sterile deionized water. Microthermoformed films were inspected under a VK-X250 confocal laser scanning microscope-based profilometer (KEYENCE) in combination with the MultiFileAnalyzer analysis software (KEYENCE) in order to determine the depth of the microwells. Microthermoformed and etched films were imaged using a Phenom ProX desktop scanning electron microscope (SEM; Thermo Fisher Scientific).

2.2. Submerged culture

The biological validation of the model was performed with A549 human lung adenocarcinoma epithelial cells, a model cell line for alveolar (epithelial) type (AT)II cells, Calu-3 human bronchial adenocarcinoma cells, a model cell line for bronchial epithelial cells, and commercial human primary alveolar epithelial cells (HPAECs). A549 cells (ATCC; CCL–185) were maintained in Dulbecco's Modified Eagle Medium (DMEM; Thermo Fisher) supplemented with 10% foetal bovine serum (FBS). Calu-3 cells (ATCC; HTB–55) were maintained in Eagle's Minimum Essential Medium (EMEM; Lonza) supplemented with 10% FBS. The media for both cell types were supplemented with 100 U/ml penicillin and 100 μg/ml streptomycin. HPAECs (Cell Biologics; delivered as passage number 3 and subcultured for another two to three passages) were cultured in a 'Complete Epithelial Cell Medium' (Cell Biologics; kit including basal medium, epithelial cell growth factor supplement, 5% FBS and 1% antibiotic-antimycotic solution) on membranes pre-coated with a 0.2% (w/v) gelatin-based solution (Cell Biologics) according to manufacturer's recommendations. The cell

cultures were incubated at 37 °C in 5% carbon dioxide. Medium was refreshed every 2–3 days. The membranes were mounted at the bottoms of 24-well plates using O-rings (ERIKS). Cells of each of the above-mentioned three types were seeded on curved and flat non-porous membranes at densities of 50,000 cells/cm^2 (D1), 5000 cells/cm^2 (D2) and 500 cells/cm^2 (D3).

2.3. Air-liquid interface culture

To investigate if the 3D culture membrane platform is suitable for ALI culture, Calu-3 cells and HPAECs were cultured with their apical side exposed to air – i.e., at an ALI – on curved and flat porous membranes mounted into CellCrown24NX culture inserts (Scaffdex Oy) for 3 weeks. The cells were seeded at density D1 and cultured submerged in culture medium for 1 week allowing them to grow confluent. After this, the medium was removed from the top compartment and consequently the culture exposed to air. The culture protocols were the same as described in the previous section. Every 2–3 days, the medium from the bottom compartment was refreshed and, in case of the Calu-3 cells, the mucus layer washed with phosphate-buffered saline (PBS; Sigma-Aldrich).

2.4. Immunofluorescence staining and confocal fluorescence microscopy

The cells were fixed with 4% paraformaldehyde in PBS for 30 min at room temperature. The fixed cells were then washed with PBS and permeabilized in 0.1% (v/v) Triton X-100 in PBS, and non-specific binding sites were blocked for 10 min in CAS-Block (Thermo Fisher Scientific). Cell nuclei and F-actin were stained with DAPI (4′,6-diamidino-2-phenylindole; 1:100; Sigma-Aldrich) for 20 min and Alexa-Fluor 647-Phalloidin (1:100; Thermo Fisher Scientific) for 30 min at room temperature, respectively. Tight junctions were stained with anti-occludin conjugated with AlexaFluor 488 (1:500; Invitrogen) overnight at 4 °C. For Calu-3 ALI culture samples, the cells were stained overnight with anti-mucin 5B (1:500; Merck). The HPAEC ALI culture samples were stained overnight with anti-aquaporin 5 (1:200; Abcam), anti-pro-surfactant protein C (1:250; Merck), anti-cytokeratin 8 (1:200; Abcam) and anti-vimentin (1:800; Dako). The samples were mounted with ProLong Gold Antifade mountant (Invitrogen Molecular Probes) (Supplementary Fig. 1). Confocal laser scanning fluorescence microscopy was performed using a Leica SP8 STED (stimulated emission depletion) microscope (Leica Microsystems). Z-stacks with 0.8–1.5 μm thick slices were acquired for all samples.

2.5. Epithelial coverage quantification

The epithelial coverage (percentage of the area covered by the formed epithelial layer) of curved and flat non-porous membranes for all three cell types seeded at all three densities (D1, D2 and D3) was quantified at days 1, 2 and 11 of culture. To this end, per sample, stained with DAPI, phalloidin and anti-occludin, images in four different spots – for curved samples containing around 20 microwells each – were taken using an ECLIPSE Ti2 inverted microscope (Nikon) with a 10× objective and analysed using the Fiji image processing software (https://fiji.sc/). For quantification purposes, the merged phalloidin and occludin images were binarized, thereby turning the cells white and the background black. The epithelial coverage was then quantified as percentage of the ratio between white and total (white plus black) area. The number of spatially independent samples (in each case mounted into a different well of a well plate) per membrane type, cell type, seeding density and time point was n = 4.

2.6. Cell density quantification

The number of cells per substrate/membrane area (‘areal cell density’) for curved and flat non-porous membranes for all three cell types seeded at density D1 was quantified at days 1, 2, 3 and 11. Per membrane sample, images of cells, stained with DAPI, phalloidin and anti-occludin, in three different spots were taken for every time point with an ECLIPSE Ti2 inverted microscope with a 40× objective and analysed using Fiji software. All images taken as a z-stack of images with step sizes of 0.8–1.5 μm were combined to create an all-in-focus image with Extended Depth of Focus (EDF), a plug-in for NIS-Elements (Nikon). The cell density was quantified and calculated by counting the cells in the area of interest (using the Cell Counter tool in Fiji) and dividing the count by the area, respectively. The number of independent samples (in each case mounted into a different well) per membrane type, cell type and time point was n = 3, the number of times the whole experiment was conducted was 2.

2.7. Quantification of neighbouring cell number

The number of directly neighbouring or ‘juxtaposed’ cells was quantified around a chosen central cell. Images of tight junctions of Calu-3 cells and HPAECs seeded at density D1 on curved and flat membranes were used to quantify the cell neighbour numbers at day 11. This was performed for 10–15 clusters of cells per sample. A549 cells were excluded from this experiment because of only partial occludin staining probably due to a reported lacking formation of functional tight junctions when grown in monolayers [16,17]. For all images, a z-stack of images was taken with step sizes of 0.8–1.5 μm and combined to create an all-in-focus image with the EDF plug-in. The number of neighbours of a selected central cell was quantified by counting the juxtaposed cells surrounding it (again using the Cell Counter tool). The number of samples per membrane type and cell type was n = 2.

2.8. Epithelial thickness measurement

The thickness of the epithelial layer formed by all three cell types seeded at density D1 on curved and flat membranes was measured at day 11. Therefore, a procedure similar to a previously reported one [18] was applied. The samples were stained with DAPI and phalloidin as described above. Images were taken as a z-stack of images with step sizes of 0.8–1.5 μm and combined to create an all-in-focus EDF image. The epithelial thickness was determined by measuring the cross-sectional projection of the samples in at least five different spots, for curved samples containing 6–8 microwells each, and with 5–20 measurements per spot, for curved samples in different locations within the microwells, using Fiji. The number of samples per membrane type and cell type was n = 3.

2.9. Proliferation and apoptosis quantification

In order to quantitatively assess proliferation and apoptosis for all three cell types seeded at density D1 on curved and flat membranes, the cells were fixed, permeabilized and blocked at days 1, 2, 3 and 11 as described above. The cells were then incubated overnight with anti-Ki-67 (1:200; Invitrogen) for proliferation and anti-cleaved caspase-3 (1:500; Cell Signaling Technology) for apoptosis. This step was followed by an 1-h incubation with an AlexaFluor 488-conjugated secondary antibody and counterstained with DAPI as explained above. Per sample, images in at least three different spots were collected for further analysis with Fiji – for curved samples of at least 3 microwells each. Cell proliferation and apoptosis were quantified by counting the cells positive for Ki-67 and cleaved caspase-3, respectively, and dividing the count by the total cell number in the image area. The number of samples per membrane type, cell type and time point was n = 3.

2.10. Epithelial permeability measurement

The diffusion of a fluorescently labelled dextran was measured to compare the barrier function of confluent cell layers on curved and flat

porous membranes after 1 week submerged culture, 3 weeks submerged culture, and first 1 week submerged and then another 2 weeks ALI (i.e., in total 3 weeks) culture. To reduce the bias by the parts of the cell layers on the non-concave surfaces between the microwells on this area-integral readout, membranes based on a hexagonal arrangement of the microwell array instead of the square array with the microwells arranged in rectangular rows and columns were employed. The membranes were mounted into the culture inserts and sealed with polydimethylsiloxane (PDMS) at their interface with the inserts/their circumference. HPAECs were seeded at density D1 and cultured as described above. Fluorescently labelled dextran with a molecular weight (MW) of 3000 (3 kDa; Invitrogen Molecular Probes) were diluted in PBS at a concentration of 1 mg/ml. From this solution, 200 μl were added to the existing or refilled culture media in the top compartment of the culture inserts in case of the submerged or temporary ALI culture, respectively, and 600 μl of medium was added to the bottom compartment. Samples were returned to the incubator and were sampled from the bottom compartment every 30 min for a period of 2.5 h. The level of fluorescence in the media was determined using a CLARIOstar plate reader (BMG LABTECH). The amount of diffused marker was calculated from a calibration curve for dextran. The apparent permeability coefficient P_{app} [19] was calculated from the linear curve fit of the data points of the amount of accumulated marker in the bottom or 'receiver' compartment at the discrete time points using the following equation:

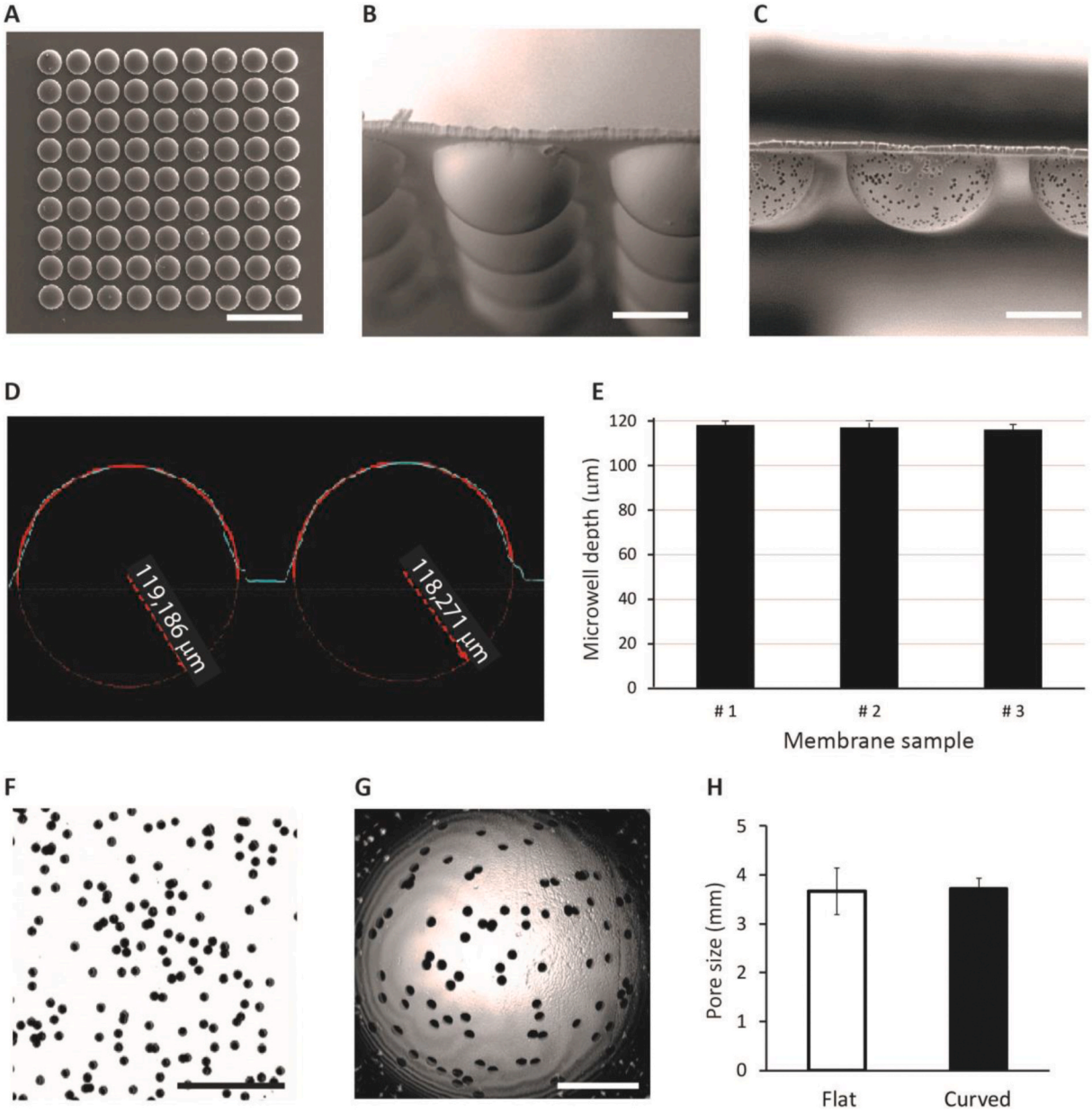

Fig. 2. Characterization of microthermoformed and ion track-etched, porous and not-etched, non-porous microwell arrays. (A) SEM image of a thermoformed membrane displaying a uniform array of hemispherical microwells (bottom/back view; scale bar: 500 μm). **(B and C)** SEM image of a close-up of non-porous and porous microwells (side views; scale bars: 100 μm). **(D and E)** Laser profilometer image (measurement from the convex bottom side/outside of the microwells) and analysis of a row of thermoformed hemispherical microwells showing uniform curvature radius and also widths or diameters of their circular upper rim (around 100 and 200 μm, respectively, on the inside, after subtracting the calculated average reduced thickness of the stretched thermoformed film; latter dimension determined by the mould used) and maximum depths (around 117 μm on the inside, again after subtracting the reduced film thickness; determined by the forming temperature and pressure applied). **(F–H)** Profilometer images and analysis of porosity of both non-thermoformed, flat and thermoformed, curved membranes, showing similar pore sizes for both types of membranes (back view; scale bars: 50 μm).

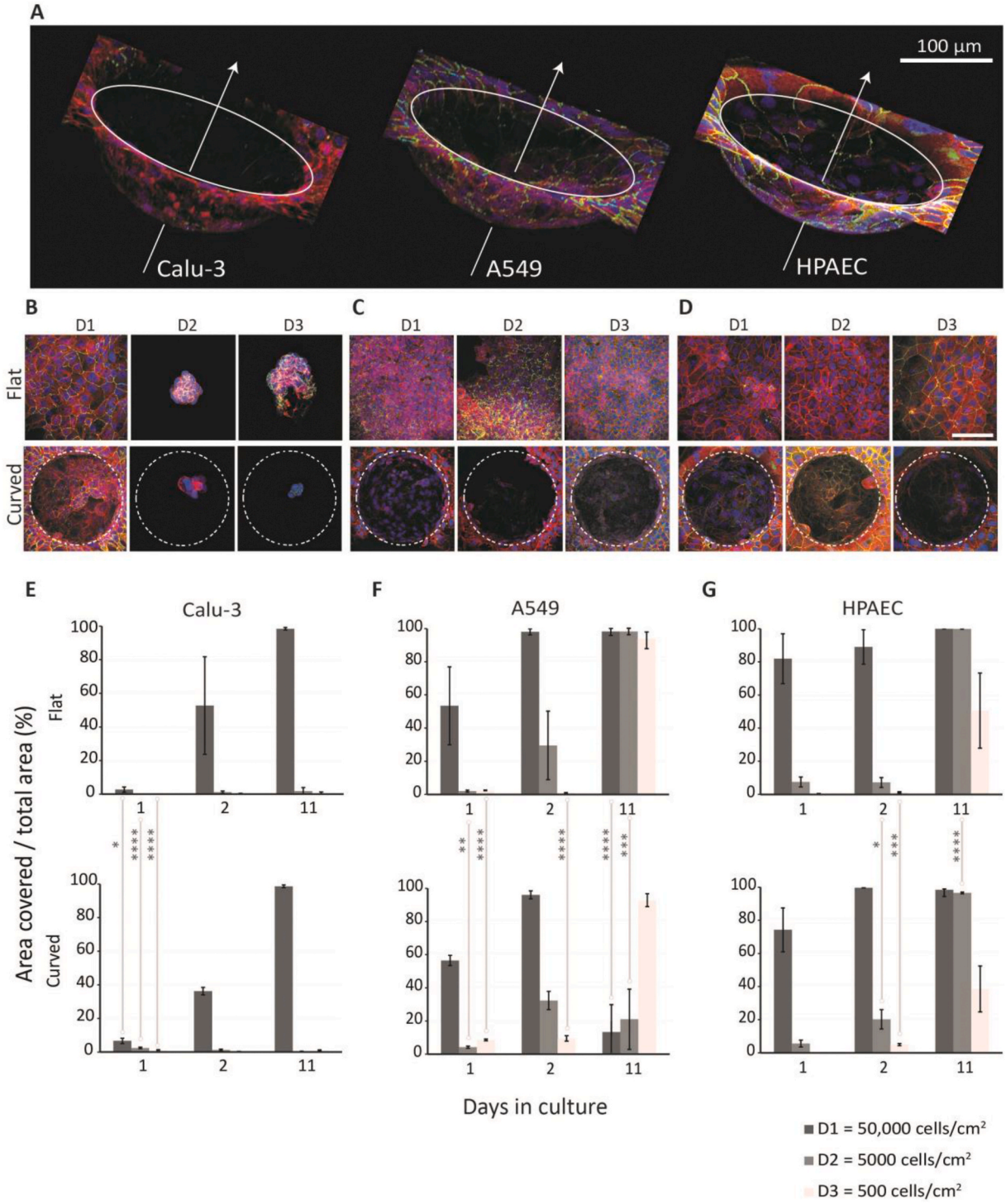

Fig. 3. Epithelialization of curved membranes. (A) 3D projections of confocal fluorescence microscopy images of Calu-3 cells, A549 cells and HPAECs cultured on thermoformed, hemispherically shaped membranes, showing cells fully lining the membranes (tilted views). Cells were stained for occludin (green), F-actin (red, phalloidin) and nuclei (blue, DAPI). **(B–D)** Confocal fluorescence microscopy images of the different cells cultured for 11 days on curved and flat membranes at different seeding densities (top views; scale bar: 100 µm; scale bar applies to all images of the subfigures). Stainings identical to Fig. 3A. **(E–G)** Quantification of membrane coverage by the different cells (meaning percentage of surface area covered with cells over total surface area) for 11 days of culture at different seeding densities on both types of membranes. *$p < 0.05$, **$p < 0.01$, ***$p < 0.001$ and ****$p < 0.0001$. (For interpretation of the references to colour in this figure legend, the reader is referred to the Web version of this article.)

$$P_{app} = \frac{dQ}{dt} \; x \; \frac{1}{A \; C_0}$$

where dQ/dt is the linear appearance rate of the dextran in the bottom compartment, A the exposed membrane area and C_0 the initial concentration of the dextran in the top or 'donor' compartment. The number of samples per membrane type and cell type was n = 3.

2.11. Statistical analysis

All data is presented as means ± standard deviation (SD). The in each case two sample groups, which always contained at least n = 3 independent (membrane) samples per experimental condition (except for the quantification of the number of neighbouring cells where the number of samples was n = 2), were analysed using a Student's t-test. Concerning statistical significance, '*', '**', '***' and '****' indicate p-values smaller than 0.05, 0.01, 0.001 and 0.0001, respectively.

3. Results

3.1. Biomimetically curved culture membranes

Bioinspired culture membranes were created by gas-assisted microthermoforming of 25 μm thin PC films. The produced membranes consist of an array of hemispherically shaped microwells each with an inner width or diameter of their circular upper rim of around 200 μm (Fig. 2A and B), determined by the mould used for thermoforming. Forming temperature and (gas) pressure were optimized resulting in hemispherical wells with around 117 μm (maximum) internal depth (Fig. 2D and E). For ALI experiments, pre-irradiated films were, as described above, microthermoformed and subsequently wet-chemically etched to obtain porous membranes (Fig. 2C, F and G). Etching resulted in pores with a diameter of 3.6 ± 0.5 μm on flat membranes, and 3.7 ± 0.2 μm on curved membranes (Fig. 2H).

3.2. Epithelialization of curved membranes and epithelial coverage

To first of all check if it is possible to grow the epithelial cells organized in monolayers on the highly curved membrane surfaces, as well as to study the effect of the seeding density on epithelial layer formation and maintenance, all three cell types were cultured on the curved non-porous membranes for up to 11 days. Thereby, also a comparison to flat membranes was drawn. The results showed that it is indeed possible for all three cell types to form epithelial monolayers on the concave surfaces (Fig. 3A). However, the epithelialization process depended on cell type and seeding density (Fig. 3B–D). Calu-3 cells formed a confluent monolayer for the highest seeding density (D1) on curved and flat membranes, which remained stable over time (Fig. 3B). However, these cells failed to form monolayers for the lower seeding densities (D2 and D3). Instead, they formed 3D cell aggregates that did not evenly (re-)populate the membrane even after 11 days in culture. A549 cells formed confluent layers on curved as well as flat membranes for all seeding densities (D1, D2 and D3) (Fig. 3C). However, for the higher seeding densities (D1 and D2), the formed epithelial layer became overgrown and over time detached, especially on curved membranes. Nevertheless, for the lowest seeding density (D3), A549 cells remained attached for the whole 11 days on the two membrane types, curved and flat ones. HPAECs fully lined both curved and flat membranes for all three seeding densities.

Concerning the percentage of area covered by cells, for all samples, an increase over time could be observed, which reflects epithelial growth (Fig. 3E–G). Calu-3 cells coverage was significantly higher on curved membranes compared to flat ones at day 1 (Fig. 3E). A549 cells showed significantly higher coverage on curved membranes for cells cultured at days 1 (D2 and D3) and 2 (D3) (Fig. 3F). However, after 11 days, due to some detachment, coverage on curved surfaces was greatly reduced. Lastly, HPAECs showed similar coverage until day 2 where, for seeding density D2 and D3, significant differences between both membrane types could be observed (Fig. 3G). At day 11, for seeding density D2, despite the significant difference in coverage for both membrane types, the epithelial layer was considered confluent.

3.3. Epithelial organization and thickness on curved membranes

To better understand how cells organize on the curved surfaces upon formation of an epithelial layer, areal cell density was quantified for cells seeded at seeding density D1 and in areas where there was no sign of cell detachment. Regardless of cell type, epithelial layers formed on curved membranes reached a higher cell density compared to flat membranes (Fig. 4A–C). This trend was present since the beginning (day 1) of the culture, but it was only significant at specific time points such as day 3 for Calu-3 cells ($p < 0.05$) and days 1 and 3 for A549 cells ($p < 0.001$) (Fig. 4A and B). On curved membranes, HPAECs consistently showed higher cell densities in comparison to flat analogues until day 3 ($p < 0.001$) (Fig. 4C). For all three cell types, at the end (day 11) of the experiment, epithelial layers formed on curved membranes tended to (still) be denser than on flat ones. To assess if curvature of the culture substrate potentially changes the filling patterns with which lung epithelial cells grow in confluent monolayers on this substrate, additionally, the number of neighbouring cells was quantified based on images of occludin stainings (Fig. 4D and E) for Calu-3 cells and HPAECs. Since A549 cells do not form defined tight junctions (see section 2.7) and also tended to overgrow (seen at day 11 when seeded at D1), we decided to not include them in this quantification. While the overall trend showed higher values of neighbouring cells for both Calu-3 cell and HPAEC layers on curved membranes compared to on flat ones, the differences between the two groups were not statistically significant.

Upon quantification of epithelial thickness, Calu-3 cells showed an approximately twofold increase in thickness on curved membranes with 13 ± 7 μm compared to flat membranes with 6 ± 1 μm (Fig. 4F and I), and A549 cells an approximate one-and-a-half-fold decrease on curved membranes with 9 ± 3 μm in comparison to flat membranes with 14 ± 2 μm (Fig. 4G and I). In case of the A549 cells, the thickness on the flat membranes was due to the cells' stacked conformation, a phenomenon that was not found on the curved membranes. Generally, on the curved substrates, the cells were able to form and maintain monolayers, which was not possible on the flat substrates. HPAEC layers reached similar thicknesses on both types of membranes with corresponding values of 8 ± 5 μm and 8 ± 2 μm for curved and flat membranes, respectively (Fig. 4H and I). The measured thickness of the alveolar cell layers is in the range reported from that of the nuclear region of (ATI) epithelial cells *in vivo* [20].

3.4. Proliferation and apoptosis on curved membranes

Cell proliferation and apoptosis was quantified for the three types of cells seeded at density D1 and cultured for 11 days on curved and flat membranes. For this purpose, we analysed the expression of the corresponding markers Ki-67 and cleaved caspase-3, respectively (Fig. 5 and Supplementary Fig. 2). According to this, Calu-3 and A549 cells presented lower rates of proliferation when cultured on curved membranes as compared to flat ones, yet only statistically significant for Calu-3 cells at day 3 (Fig. 5A and B). HPAECs showed a confluence-dependent response. Before reaching confluence, at days 1 and 2, HPAECs on curved membranes had higher rates of proliferation, but also higher rates of apoptosis (Fig. 5C and F) than on flat membranes. After reaching confluence, at days 3 and 11, this was reversed so that now cells on the same, curved membranes had lower levels of proliferation and apoptosis. Calu-3 cells showed consistently higher rates of apoptosis on curved membranes in comparison to flat ones (Fig. 5D). A549 cells had low apoptosis rates at all days on both membrane types (Fig. 5E). Generally, for all cell types and at every time point, apoptosis levels on

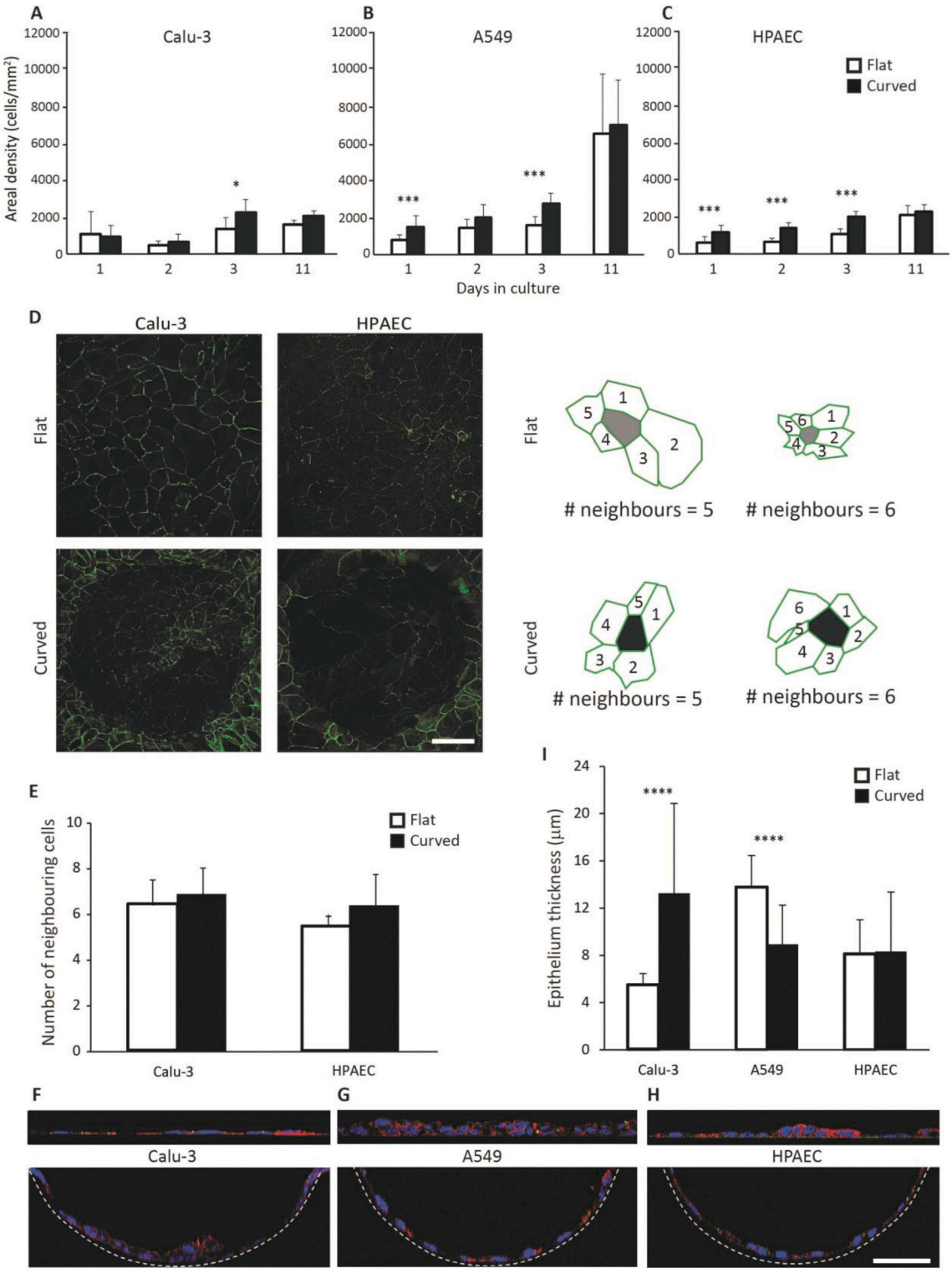

Fig. 4. Epithelial organization on curved membranes. (A–C) Quantification of areal cell density of Calu-3 cells, A549 cells and HPAECs cultured on curved and flat membranes up to 11 days at a seeding density of 50,000 cells/cm^2. **(D)** Confocal fluorescence images of Calu-3 cells and HPAECs cultured for 11 days on curved and flat membranes showing tight junctional network (top views; occluding, green; scale bar: 50 μm; scale bar applies to all images of the subfigure). **(E)** Neighbouring cells quantified from occluding staining (as depicted) of Calu-3 cells and HPAECs cultured on curved and flat membranes for 11 days at a seeding density of 50,000 cells/cm^2. *$p < 0.05$, **$p < 0.01$, ***$p < 0.001$ and ****$p < 0.0001$. **(F–H)** Confocal fluorescence images of Calu-3 cells, A549 cells and HPAECs cultured on curved and flat membranes, showing topological differences between epithelial layers (cross-sectional views; scale bar: 50 μm; scale bar applies to all images of the subfigures). Cells were stained for occludin (green), F-actin (red, phalloidin) and nuclei (blue, DAPI). **(I)** Epithelial thickness quantified from cross-sectional confocal images of Calu-3 cells, A549 cells and HPAECs cultured for 11 days at a seeding density of 50,000 cells/cm^2 on curved and flat membranes. (For interpretation of the references to colour in this figure legend, the reader is referred to the Web version of this article.)

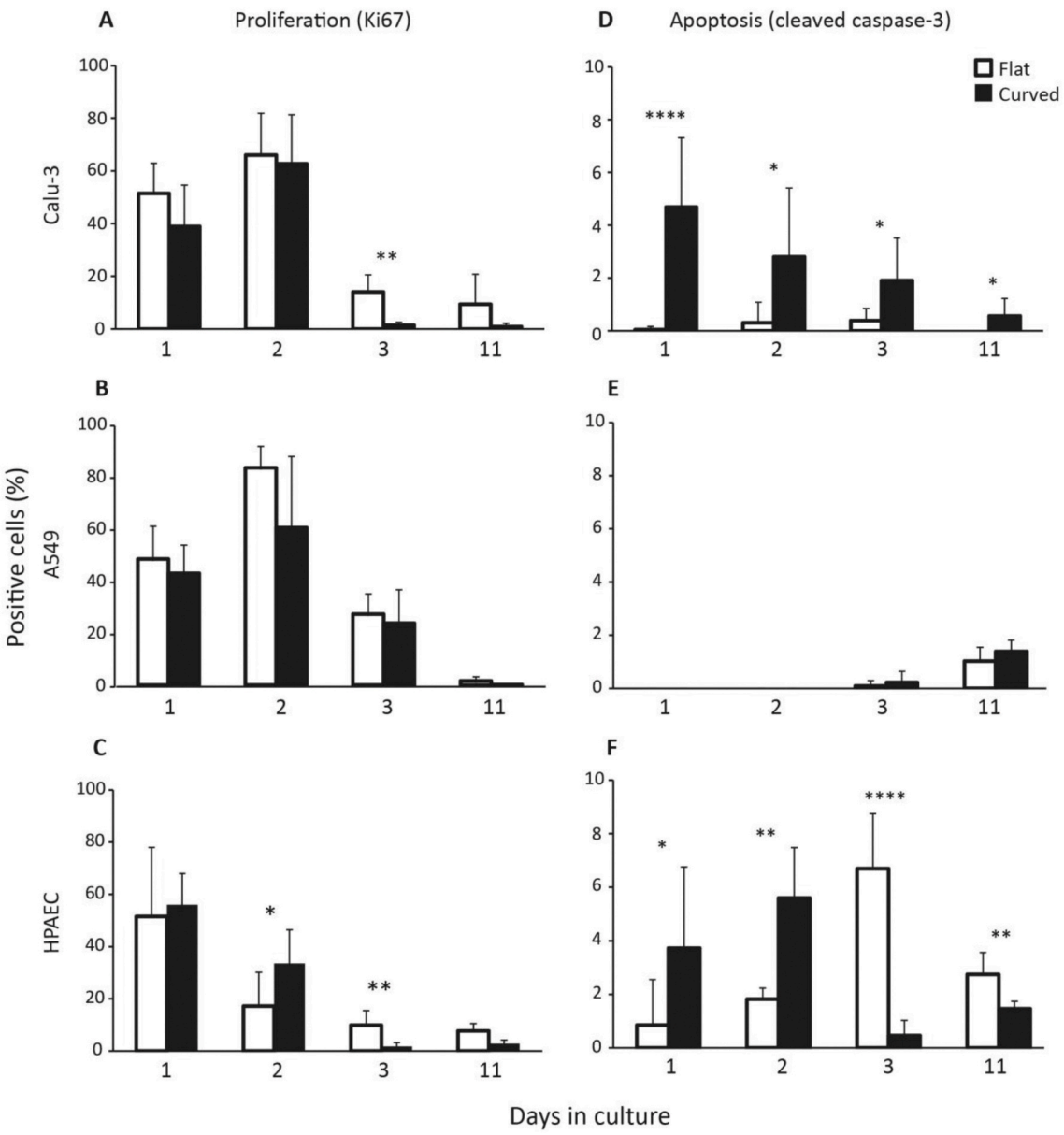

Fig. 5. Cell proliferation and apoptosis under curved regimes. (A and D) Calu-3 cells, **(B and E)** A549 cells and **(C and F)** HPAECs cultured on curved and flat membranes were stained for Ki67 (proliferation marker) and cleaved caspase 3 (apoptosis marker) and the respective expression (meaning percentage of number of marker-positive cells over total number of cells) was quantified. *p < 0.05, **p < 0 .01, ***p < 0.001 and ****p < 0.0001.

curved membranes were around or below 5% (Fig. 5D–F).

3.5. Epithelial permeability on curved membranes

To assess the barrier integrity and function of layers from HPAECs on curved and flat membranes, we measured the diffusion of a 3000 MW dextran through these layers. The measurement results showed a similar permeability of the curved and the flat epithelial layers with a (non-significant) trend towards lower values, meaning tighter barriers, for the curved layers for all culture conditions and durations (Fig. 6). The measurements also showed similar permeability between the different conditions and durations with a (again non-significant) trend now towards higher values for the longer culture durations and ALI culture. The values are 2.4 and 1.7 $\times$ 10^{-7} cm/s for 1 week submerged culture, 4 and 3.1 $\times$ 10^{-7} cm/s for 3 weeks submerged culture, and 30 and 7.2 $\times$ 10^{-7} cm/s for 1 week submerged culture followed by 2 weeks ALI culture, in each case for flat and curved substrates, respectively. Significantly higher permeability values, 10 and 8.8 $\times$ 10^{-5} cm/s ($p = 0.00129$ and 0.00014), respectively, resulted from the same substrate types but without cells cultured on them.

3.6. Air-liquid interface culture on curved membranes

The feasibility of establishing an ALI culture on curved membranes was investigated with Calu-3 cells and HPAECs. Thermoformed membranes were mounted into the culture inserts, allowing the cells to be cultured air-exposed. After 1 and 3 weeks at the ALI, the Calu-3 layer was analysed for thickness (Supplementary Fig. 3) as well as for mucus production by staining for mucin 5B (Fig. 7A). Regarding morphological aspects of the engineered epithelial layers, curved membranes presented epithelial thicknesses of 17 $\pm$ 6 μm and 11 $\pm$ 3 μm at 1 and 3 weeks of ALI culture, respectively. Flat membranes presented cell layer thicknesses of 26 $\pm$ 6 μm and 31 $\pm$ 3 μm at 1 and 3 weeks at the ALI, respectively. This means that both at week 1 and 3 the curved epithelial layers were significantly thinner than the flat ones. Over time, the thickness of curved cell layers significantly decreased while flat layers

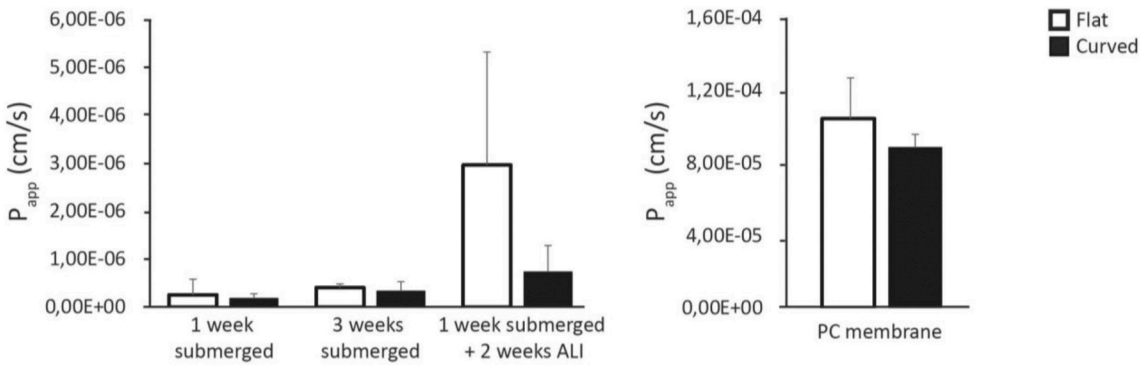

Fig. 6. Permeability of curved epithelial layers. (Epithelial) permeability (P_{app}) was calculated from passive diffusion of a fluorescently labelled 3000 MW dextran for **(left)** HPAECs grown submerged for 1 week, submerged for 3 weeks, and first submerged for 1 week and then at the ALI for another 2 (i.e., in total for 3 weeks) weeks on curved and flat membranes and **(right)** the same membrane types but without cells grown on them. *p < 0.05, **p < 0.01, ***p < 0.001 and ****p < 0.0001.

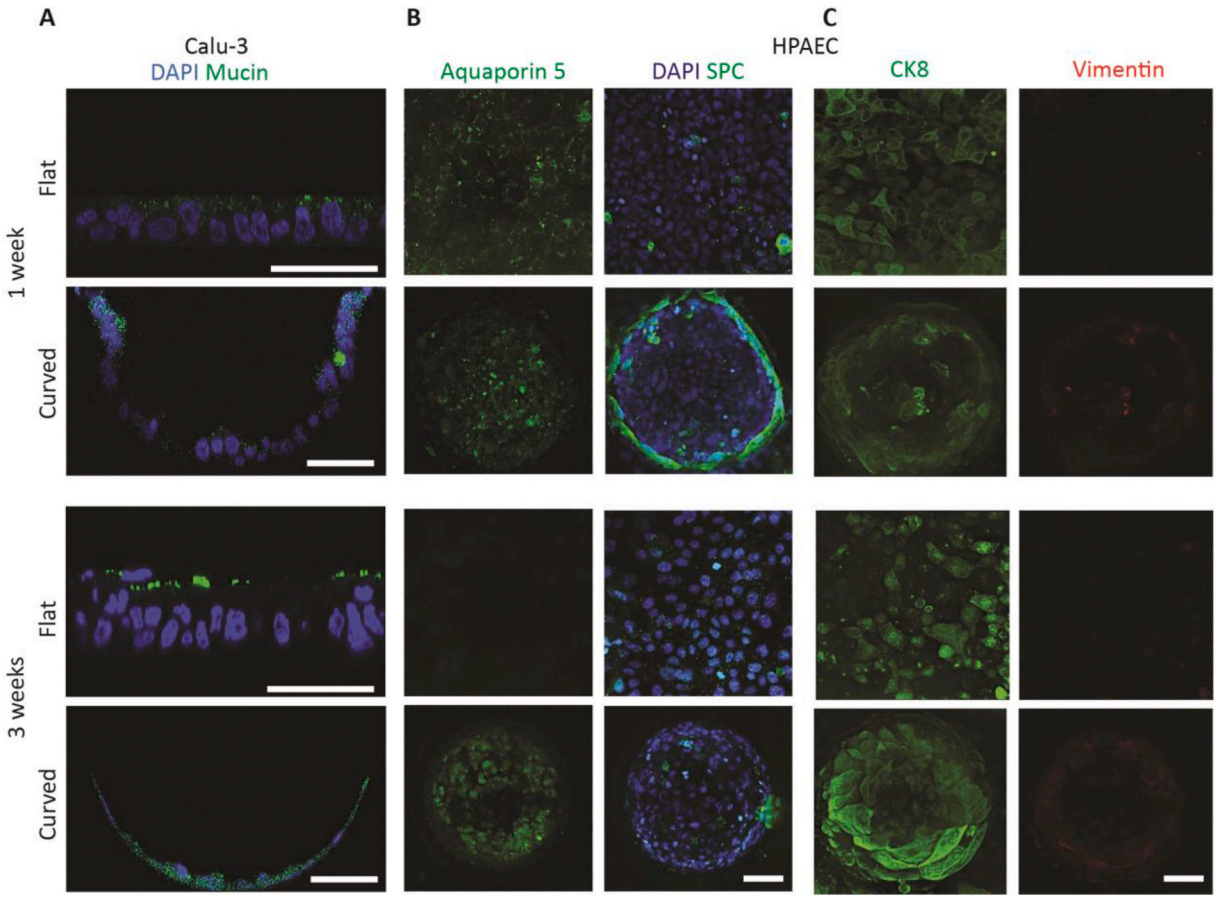

Fig. 7. ALI culture on epithelialized curved membranes. (A) Fluorescence confocal images of Calu-3 cells cultured at the ALI for 1 and 3 weeks on curved and flat membranes (cross-sectional views; scale bars: 50 μm). Cells were stained for mucus (green, mucin 5B) and nuclei (blue, DAPI). **(B)** Fluorescence confocal images of HPAECs cultured at the ALI for 1 and 3 weeks on curved and flat membranes (top views; scale bar: 50 μm; scale bar applies to all images of the subfigure). Cells were stained for an ATI marker (green, aquaporin 5, left double column), an ATII marker (green, surfactant protein c, right double column) and nuclei (blue, DAPI, right two columns). **(C)** Fluorescence confocal images of HPAECs cultured at the ALI for 1 and 3 weeks on curved and flat membranes (top views; scale bar: 50 μm; scale bar applies to all images of the subfigure). Cells were stained for an epithelial marker (green, CK8) and EMT (red, vimentin). (For interpretation of the references to colour in this figure legend, the reader is referred to the Web version of this article.)

increased in thickness. Regarding the mucin 5B expression, this was diffuse on curved membranes, while on flat ones it appeared apically localized. HPAECs grown at an ALI were examined for ATI and ATII markers. Results revealed that these cells had a weak expression of aquaporin 5 and pro-surfactant protein C (pSPC) (Fig. 7B). pSPC was expressed in some cells across the entire surface, seemingly more prominent on the edge of curved membranes at week 1. Regarding epithelial-(to-)mesenchymal transition (EMT), there were no signs of this transition behaviour occurring over time, except for a very weak but not completely absent staining of vimentin (Fig. 7C). At the same time, cells were widely positive for cytokeratin 8 (CK8; Fig. 7C). The expression of this marker became more intense on curved samples after 3

weeks of culture. A549 cells were excluded from this experiment as well as from the previous one (see section 3.5.) because of their leaky nature upon barrier formation [21] and propensity for EMT [22].

4. Discussion

Current ALI cell culture models of the pulmonary alveoli or the small airways such as based on conventional culture inserts but also on more advanced organs on chips [23–25] are only to a limited extent representative of the corresponding anatomical structures and consequently their physiology. To the best of our knowledge, there are currently no ALI alveolar models including the preservation of the lung acinar microanatomy. (Lung) organoid models increasingly also drawing the interest of lung researchers [26] display at least in part such a complex architecture. However, their hardly accessible apical lumens are not air but fluid filled [27]. Along with efforts to mimic the native curvature of tissues in *in vitro* models generally [3], curvature is also considered an integral part of models of other acinar tissues apart from lung [18].

In the present study, first steps were taken towards the (re)creation of a more realistic, 3D *in vitro* model of the alveolar tissue imitating its curved architecture. The model is based on ion track-etched membranes as one of the most relied-on cell culture substrates, however not in their commonly applied flat form. Instead, the membranes are 3D shaped into arrayed hemispherical microwells, geometrically resembling key features of an open(ed) adult alveolar sac. On these bioinspired membranes, we have successfully demonstrated the formation, the growth and a first characterization of curved layers from A549 cells, Calu-3 cells and HPAECs.

As previously reviewed, engineering substrates with precise and smooth out-of-plane-curved structures at a cell-relevant, mm- and μm-scale can be challenging [3]. Methods that allow the fabrication of such curved structures include mechanical micromachining [28], (photo) lithography followed by isotropic etching [29] or thermal reflow of photoresist [18], grey-scale lithography [30], laser (micro)machining [31], alpha-particle radiation and subsequent chemical etching of the latent particle tracks [32], microtunable mould-derived techniques [33], stereolithography and two-photon laser lithography [34]. Another method is the one presented in this paper. Compared to the methods listed above, it allows small-scale curvature in conjunction with thin-walled porous (micro)structures and therefore enables substrates that can be applied in ALI culture, being essential for many tissue barrier models. During the free-forming process employed to shape the membranes, the film does not touch the mould in the areas where the curved microwells are formed. This prevents the surface roughness of the mould to be partially imprinted into the surface of the film, potentially compromising later microscopic imaging and also cell growth on the corresponding side of the membrane in case of epithelial-endothelial co-culture.

The curved membranes are made from PC, which is a standard cell culture material and used in conjunction with ion track membranes in culture inserts in general and particularly for ALI culture of alveolar cells [35]. PC, however, is rather stiff compared to lung tissue. The elastic modulus of PC is at the GPa-level, whereas the one of lung tissue is in the few kPa-range [36]. Therefore, for further development of the model, it would be worth considering other, more flexible polymer formulations such as poly(trimethylene carbonate) (PTMC) [37]. This would also allow to the implementation of cyclic stretching by means of corresponding actuators. In conjunction with a (bioinert) mesh-/web-type support similar to the mould for forming the microwell arrays, a controlled and identical periodic out-of-plane dilation of each individual microwell of an array mounted into the support and with it of the cell monolayer lining and adhering to the curved microwell surface could then be accomplished (similar to Supplementary Figs. 4 and 5). In its capacity as a polymer moulding process, microthermoforming as the basis of the process for the fabrication of the curved membranes allows the realization of many other designs and the application of many other thermoplastic (biocompatible) materials [11]. Again due to the fact that the material is processed under conditions of material coherence, the forming can also be combined with other processes for the production of porous membranes, as a prerequisite for ALI culture, such as laser drilling [38], phase separation or electrospinning [39]. The ion track-etched membranes are in the first instance a structural material for a cell culture substrate possessing a basic bio- or cytocompatibility. This can be further improved, as it is already conducted routinely for flat culture membranes and can be similarly performed in case of the curved ones, by the application of extracellular matrix protein-based coatings such as from gelatin, collagen, fibronectin or laminin. Altogether, this will allow the provision of dedicated microcurved membrane environments also for *in vitro* models of other epithelial and/or endothelial tissue barriers such as of the bronchioles, renal tubules, intestinal villi, or lymph or blood vessels. In case that models of tubular barriers based on curved membranes shall be subjected to physiological flow, the microthermoforming technology would also allow to create perfusable lumens (with circular cross-sections) by joining and sealing mirror-inverted film or membrane microchannels with (hemispherical cross-sections) as similarly shown by us [40].

The curved membrane engineered in this study provides an increased surface area (on the same base area) for more efficient gas exchange, which should support a physiologically more accurate lung model, also as part of multi-organ model systems [41]. Also, because of its biomimetic topography, the model should be more realistic in conjunction with deposition of therapeutic aerosols, cigarette smoke or fine dust from technical sources after corresponding exposure compared to flat models. The microwells with circular upper rims were arranged in rectangular rows and columns as similarly used in high-throughput screening applications [42]. For this reason, in addition to the smaller rounded, convex ridges between two adjacent wells, larger flat regions still exist in between every four wells. In conjunction with studies on the impact of the concave curvature inside the wells on cells, cells on these non-concave surfaces can be assumed to bias the outcome of analyses of cellular lysates by biomolecular techniques such as Western blotting and polymerase chain reaction [3]. Therefore, in the current study, characterization of the bioinspired lung model was mainly based on microscopic imaging. A potential solution to reduce planar surface area and further increase curved and therewith total surface area is a redesign towards a hexagonal, honeycomb-type arrangement of the microwells. This configuration with increased similarity to the original tissue can be even further improved in terms of total surface area and imitation of the tissue by designing the upper rims of the wells in a related hexagonal fashion, as already shown by us in conjunction with topographically defined artificial microenvironments [14] (Supplementary Fig. 4).

Cell source selection is important to investigate the applicability and translatability of our platform. For this study, A549 cells were selected as they are a model cell line for ATII cells. A549 cells share some characteristics with human ATII cells [43] and hence have been used in many corresponding studies. Calu-3 cells are a model cell line for bronchial cells, with reported mucus secretion. Even if not being of alveolar origin and if the curvature types and diameters experienced by epithelial cells in the bronchioles are different from those of the alveoli, Calu-3 cells were chosen as they are one of the few respiratory cell lines that form tight junctions *in vitro* [8]. For the same reason, Calu-3 cells have been widely used in airway epithelial barrier studies [44]. The HPAECs used in this study were selected to add more relevance to the study by using a primary cell, but also to gain more flexibility and comparability in the study, not so dissimilar from when using a cell line. The HPAECs have been already used in a number of studies [45–48]. The fact that these cells have been frozen, thawed and passaged a few times sets them back compared to freshly isolated primary human alveolar epithelial cells (AECs). This is also evident from the staining patterns of ATI and ATII markers used. Despite various challenges associated with culturing freshly isolated primary human AECs as part of corresponding *in vitro* models such as limited availability of fresh human peripheral

lung tissue, limited proliferation capacity [49], extensive cell death within the first few days in culture (60–70%) [50] and changes in ATI-ATII ratio over time [51], in most cases, they are still the preferred cell source in these type of applications. Further advances in the development of primary AEC culture and the derivation of human AECs from embryonic stem cells and induced pluripotent stem cells (iPSCs) [52] might address these challenges in the medium term.

For the establishment of a functional barrier, the formation of a defect-free confluent cell monolayer is essential. Establishing such a monolayer from the different lung epithelial cells on the strongly curved membranes, as successfully demonstrated in this study, is a non-trivial process for three main reasons [3]. The first one is related to the technical step of cell seeding. When inoculating cells into the microwells just by gravity seeding, they mainly concentrate in the deepest parts of the wells. To support, for example, the uniform endothelialization of microfluidic channels with curved, circular cross sections, inoculation of the cells by infusion was followed by (rocking and/or) rotation of the culture substrate [53,54]. In this study, all three different cell types were able to properly line and fully cover the curved membranes following gravity seeding without any additional means. However, epithelialization of curved surfaces was found to be cell type- and seeding density-dependent. While A549 cells and HPAECs formed confluent layers for all three tested seeding densities, for Calu-3 cells this was only possible for the highest density (D1); otherwise, they formed aggregates.

The second reason for the epithelialization being a non-trivial process relates to a counteracting type of cell migration. If the substrate design allows so, as in case of our arrayed microwells with flat regions between them, cells may on average avoid the concave regions by migrating out of the wells or prefer the flat regions (over the curved ones) by migrating into the regions between the wells. This was similarly shown for L929 fibroblasts and human mesenchymal stromal cells (hMSCs) cultured on arrays of (hemi)spherical microwells from PDMS with dimensions similar to the ones in our study [31]. In the majority of the conditions where at a certain time point there has been a full coverage of the curved (and also flat) regions of the membranes by confluent monolayers with defined tight junctions, there was obviously no avoidance of curvature, at least not on the (tissue-)level of the finally formed epithelial layers. This might be the result of a predisposition of the cells used in this study for small-scale concave curvature. Our findings are in line with the ones of others culturing epithelial cells on such surfaces mimicking the acinar-type anatomy of their native microenvironments [18,55]. To more efficiently populate curved luminal substrates or scaffolds with epithelial or endothelial cells, but also to better understand tissue repair under such framework conditions, more studies on cell migration on the corresponding concave surfaces [56] are needed.

The third reason is in relation to tissue detachment. The equilibrium between substrate curvature, cellular contractility within a tissue adhering to the curved substrate and strength of ECM-mediated cell-substrate adhesion determines if the tissue remains attached or detaches [57]. In case of too small curvature radii, high contractile forces and low adhesive strength, tissues, partly or fully, detach from the curved surface. As shown, A549 cells properly lined the curved membranes for all tested seeding densities, but for the highest seeding density, they detached from the substrate once overgrown beyond monolayer. This phenomenon was similarly observed in another study, there in conjunction with solid mechanical und surface tension fluid mechanical stress [58].

Cells within an epithelium systematically change their numbers, size and shape as an organ develops, an injury heals or a carcinoma spreads [59]. Such a collective cellular system is dynamic and can transition from an unjammed, fluid-like state to a jammed, solid-like state. Unjammed and jammed epithelia differ in aspects such as cell migration, cell density or crowding [60,61], and cell shape and shape variability [59]. In jammed epithelia, higher cell density leads to limited configurational options, with cell movements being constrained and rearrangements among neighbouring cells being slowed down. In our study, it was observed that curved membranes resulted in higher areal density or crowding of cells, which, according to the afore-cited corresponding studies, might suggest that these cells were further jammed than the ones on flat substrates. Further investigations should focus on cell migration and motility on curved surfaces as well as on quantifying other parameters such as the 'shape index' [62] to potentially confirm that curvature contributes to cell jamming. Recently, cell jamming has been investigated in conjunction with diseases such as cancer [63,64] and asthma [65], which would broaden the applicability of our platform. The study of epithelial topology shows a prevalence of pentagonal, hexagonal and heptagonal cell shapes in order to minimize surface energy or maximize space filling [66]. Our study on cell neighbour numbers provided similar results. Calu-3 cells and HPAECs had on average five to six neighbours, with a small variability, and therefore were approximately pentagonal and hexagonal cells. Although not being statistically significant, the trend indicates that curved substrates lead to more cell neighbours than flat ones.

In our study, we investigated proliferation and apoptosis during formation and growing of the epithelial layer. The results showed cell type-dependent distinct values for curved and flat membranes. The lung epithelial cell lines (Calu-3 and A549) consistently presented lower rates of proliferation and higher rates of apoptosis on curved membranes compared to flat ones. In another study, it was also reported that the concave substrate curvature of spherical microwells from PDMS similarly sized as the ones in our study suppresses the proliferation of cells, though of very different ones, L929 fibroblasts and hMSCs [31]. The primary AECs in our study showed higher rates of proliferation and apoptosis on curved membranes at earlier time points, and lower proliferation and apoptosis rates after reaching confluence.

From a technical perspective, our biomimetically curved membranes can easily be integrated in culture inserts. This makes it possible to culture cells first submerged and then air-exposed, which is a valuable tool in pulmonary research as ALI cultures mimic a more realistic lung environment and enable airway epithelial cells to proliferate and differentiate *in vitro* [52]. From a biological perspective, Calu-3 cells and HPAECs cultured at an ALI remained viable up to 3 weeks, which validates this platform as a suitable candidate for long-term culture experiments. Assessment of permeability of HPAEC layers based on the diffusion of a 3000 MW dextran showed similarly low values for permeability mainly in the 10^{-7} m/s range for shorter and longer submerged and ALI culture on curved and flat epithelial layers, with a trend towards higher values at the ALI, as similarly reported for other lung epithelial cells [44,67]. For the same substrate types but without cells, significantly higher values mainly in the high 10^{-5} to low 10^{-4} cm/s range could be shown. Interestingly, it was reported that salivary gland epithelial cells grown on curved substrates presented higher expression and stronger apical localization of the tight junction protein occludin, which suggests that a curved conformation might facilitate tight junction assembly between cells [18]. One could speculate that the same occurs with lung epithelial cells, therefore contributing to a stronger corresponding barrier. Further investigations need to be carried out to better understand the mechanism behind a potential improvement of barrier function on curved culture surfaces.

In another study, Calu-3 cell layers grown on flat substrates at an ALI for 11 days presented layer thicknesses of 20–45 μm [44]. Our results for flat membranes for 1 and 3 weeks of culture fall within this value range. However, the corresponding results for our curved samples are below this range. At the end of culture week 3, the thickness of the curved epithelial layers was only roughly one third of that of the flat ones. Also in this case, the effect of the curved surfaces needs further investigation.

In mammalians, ATII cells are mainly located in the corners where neighbouring alveoli meet [68,69]. Therefore, we investigated whether in an ALI alveolar model based on our biomimetically curved membranes populated with HPAECs this cellular distribution could be found in a similar place, possibly due to the existence of a certain surface

curvature in a specific location. For this purpose, we searched for the presence of aquaporin 5-positive ATI- and pSPC-positive ATII-like cells in the curved microwells. The HPAECs were found to have a weak expression of both aquaporin 5 and pSPC. The latter was observed more prominently expressed in the region around the inflexion point between the concave and the convex surfaces of the microwells and their rims, respectively, there creating pSPC-positive cell rings. However, this configuration was lost after 3 weeks. In another study, primary adult mouse ATII cells were encapsulated in 200 μm wide lobe-type microwells in the form of overlapping circular cylindrical structures with flat bottoms, created in a layer of a cell-adhesive hydrogel and closed with another hydrogel layer [70]. In these microwells, intermediate phenotype cells staining positive for both ATI and ATII markers where shown to reside mainly near the tops of the wells, whereas a population of ATII cells resided primarily lower down in the wells. However, the cell aggregates in the lobe-type wells do not match the spatial arrangement of alveolar phenotypes observed *in vivo*. In our respective experiments, more similar to the situation *in vivo*, an ATII-like population was located near the rim of the microwells at least for 1 week of culture. This preliminary data suggests an additional confirmation and a further investigation of the potential role of substrate curvature in ATII differentiation. Curvature, more specifically the convex in-plane curvature of sinusoidal cell-adhesive islands on a planar substrate [71] and the convex surface curvature of cylindrical fibres or wires, was reported as an inducer of EMT. Thereby, the curvature influences migration patterns to shift from a collective behaviour being typical for epithelial cells to individual cell movements as seen with mesenchymal cells. In this context, it is important to note that the absence of EMT of alveolar epithelial cells on the bioinspired membranes is a prerequisite for their use in corresponding models, for example, in drug testing. HPAECs showed no signs of EMT on the curved membranes as the mesenchymal marker vimentin was factually not expressed. At the same time, the epithelial marker CK8 was strongly expressed on the identical substrate type for up to 3 weeks at the ALI.

5. Conclusions

Here, we propose a more realistic culture environment for lung alveolar cells based on biomimetically curved track-etched membranes, restoring the geometry of the cells' native microenvironment. The curved membranes were created by a combination of 3D micro film (thermo)forming and ion track etching. We could successfully demonstrate the formation, growth and a first characterization of confluent layers of A549 cells, Calu-3 cells and HPAECs on membranes shaped into an array of hemispherical microwell structures. We determined the appropriate seeding conditions to completely line the curved walls of the microwells with confluent epithelial layers, which in case of layers of Calu-3 cells and HPAECs could be cultured for up to 3 weeks at the ALI. Air-exposed culture was enabled by the thin porous walls of the curved membrane microstructures. The characterization concerning membrane epithelialization, areal cell density of the formed epithelial layers, their cross-sectional morphology and thickness, and proliferative and apoptotic ratios revealed significant differences in the response of the cells on and to the curved membranes compared to the flat ones, and regarding barrier function the same low permeability for cell layers on both substrate types.

The above-described achievements towards the creation of a more realistic, 3D *in vitro* model of the alveolar tissue imitating its curved architecture can only represent the first steps in this direction. Further efforts must follow, including validation of the model with primary human AECs freshly isolated or derived from iPSCs, and gene-level phenotypic characterization of the cells of the model. This might be accompanied by endeavours in conjunction with next levels of biomimicry, such as a polygonal arrangement and shape of the microwells and their rims, respectively, as well as soft tissue-like elasticity or flexibility of the membrane material. But already on the basis of ion track-etched membranes as one of the most trusted cell culture substrates, the versatility of the micromoulding-based process for the fabrication of the curved membranes presented in this paper will allow the provision of dedicated 3D membrane environments also for *in vitro* models of other epithelial and/or endothelial barrier tissues. Examples are models of the bronchioles, renal tubules, intestinal villi, or lymph or blood vessels. A better understanding of the assumed beneficial role of curved culture substrates over their flat counterparts in such membrane-based tissue barrier models on the establishment and maintenance of more functional and physiological barriers *in vitro* could change the design and performance of such models in a multitude of applications in the not too distant future.

CRediT authorship contribution statement

D. Baptista: Formal analysis, Investigation, Methodology, Visualization, Writing - original draft, Writing - review & editing. **L. Moreira Teixeira:** Methodology, Writing - original draft, Writing - review & editing. **Z. Tahmasebi Birgani:** Methodology, Writing - review & editing. **S. van Riet:** Writing - review & editing. **T. Pasman:** Writing - review & editing. **A. Poot:** Funding acquisition, Writing - review & editing. **D. Stamatialis:** Funding acquisition, Writing - review & editing. **R.J. Rottier:** Funding acquisition, Writing - review & editing. **P.S. Hiemstra:** Funding acquisition, Writing - review & editing. **P. Habibović:** Funding acquisition, Writing - review & editing. **C. van Blitterswijk:** Funding acquisition, Writing - review & editing. **S. Giselbrecht:** Conceptualization, Funding acquisition, Methodology, Supervision, Writing - review & editing. **R. Truckenmüller:** Conceptualization, Funding acquisition, Methodology, Supervision, Writing - original draft, Writing - review & editing.

Declaration of competing interest

The authors declare the following financial interests/personal relationships that may be considered as potential competing interests: R. T. and S. G. are founders, shareholders and managing directors of the company 300MICRONS GmbH active in the field of 3D cell culture solutions.

Acknowledgements

D. B., S. v. R. and T. P. acknowledge financial support by the Lung Foundation Netherlands (project 'Microengineered 3D analogues of alveolar tissue for lung regeneration'; no. 6.1.14.010), D. B. and L. T. by the European UnionHorizon 2020 European Research Council Advanced Grant (project 'ORCHESTRATE – Building complex life through self-organization: from organ to organism'; ID 694801), P. H., C. v. B., S. G. and R. T. by the Dutch province of Limburg (program 'Limburg INvesteert in haar Kenniseconomie/LINK'; nos. SAS-2014-00837 and SAS-2018-02477), Z. T. B. by the European Union/Interreg Flanders-The Netherlands (project 'Biomat on microfluidic chip', no. 0433), and P. H., S. G. and R. T. by the Gravitation Program of the Netherlands Organisation for Scientific Research (project 'Materials-driven regeneration: Regenerating tissue and organ function with intelligent, life-like materials'; no. 024.003.013).

Appendix

3D	Three-dimensional
AEC	Alveolar epithelial cell
ALI	Air-liquid interface
AT(I/II)	Alveolar type (I/II)
CK8	Cytokeratin 8
COPD	Chronic obstructive pulmonary disease
DAPI	4′,6-diamidino-2-phenylindole

DMEM	Dulbecco's Modified Eagle Medium
ECM	Extra cellular matrix
EDF	Extended Depth of Focus
EMEM	Eagle's Minimum Essential Medium
EMT	Epithelial-(to-)mesenchymal transition
FBS	Foetal bovine serum
hMSC	Human mesenchymal stromal cell
HPAEC	Human primary alveolar epithelial cell
iPSC	Induced pluripotent stem cell
MW	Molecular weight
P_{app}	Apparent permeability coefficient
PBS	Phosphate-buffered saline
PC	Polycarbonate
PDMS	Polydimethylsiloxane
PLA	Polylactic acid
pSPC	Pro-surfactant protein C
PTMC	Poly(trimethylene carbonate)
SEM	Scanning electron microscope
STED	Stimulated emission depletion

Appendix A. Supplementary data

Supplementary data to this article can be found online at https://doi.org/10.1016/j.biomaterials.2020.120436.

References

[1] E.S. Russell, Form and function: a contribution to the history of animal morphology, Nature 98 (1916) 306–307.
[2] D.E. Ingber, Mechanical control of tissue growth: function follows form, Proc. Natl. Acad. Sci. U.S.A. 102 (2005) 11571–11572.
[3] D. Baptista, et al., Overlooked? Underestimated? Effects of substrate curvature on cell behavior, Trends Biotechnol. 37 (2019) 838–854.
[4] S.J.P. Callens, et al., Substrate curvature as a cue to guide spatiotemporal cell and tissue organization, Biomaterials 232 (2020) 119739.
[5] R. Spohr, Ion Tracks and Microtechnology. Principles and Applications, Vieweg, Braunschweig, 1990.
[6] B.M. Wiebe, H. Laursen, Human lung volume, alveolar surface area, and capillary length, Microsc. Res. Tech. 32 (1995) 255–262.
[7] M. Ochs, et al., The number of alveoli in the human lung, Am. J. Respir. Crit. Care Med. 169 (2004) 120–124.
[8] K.A. Foster, et al., Characterization of the Calu-3 cell line as a tool to screen pulmonary drug delivery, Int. J. Pharm. 208 (2000) 1–11.
[9] K.F. Chung, I.M. Adcock, Multifaceted mechanisms in COPD: inflammation, immunity, and tissue repair and destruction, Eur. Respir. J. 31 (2008) 1334–1356.
[10] A.J. Miller, J.R. Spence, In vitro models to study human lung development, disease and homeostasis, Physiology 32 (2017) 246–260.
[11] R. Truckenmüller, et al., Thermoforming of film-based biomedical microdevices, Adv. Mater. 23 (2011) 1311–1329.
[12] S. Giselbrecht, et al., 3D tissue culture substrates produced by microthermoforming of pre-processed polymer films, Biomed. Microdevices 8 (2006) 191–199.
[13] A. Linhartová, et al., A proposed alveolar model for adult human lungs: the regular dodecahedron, Anat. Rec. 214 (1986) 266–272.
[14] R. Truckenmuller, et al., Fabrication of cell container arrays with overlaid surface topographies, Biomed. Microdevices 14 (2012) 95–107.
[15] R. Truckenmüller, et al., Flexible fluidic microchips based on thermoformed and locally modified thin polymer films, Lab Chip 8 (2008) 1570–1579.
[16] A.J. Carterson, et al., A549 lung epithelial cells grown as three-dimensional aggregates: alternative tissue culture model for Pseudomonas aeruginosa pathogenesis, Infect. Immun. 73 (2005) 1129–1140.
[17] H. Ren, et al., An optimised human cell culture model for alveolar epithelial transport, PloS One 11 (2016), e0165225.
[18] D.A. Soscia, et al., Salivary gland cell differentiation and organization on micropatterned PLGA nanofiber craters, Biomaterials 34 (2013) 6773–6784.
[19] S. Berggren, et al., Characterization of jejunal absorption and apical efflux of ropivacaine, lidocaine and bupivacaine in the rat using in situ and in vitro absorption models, Eur. J. Pharmaceut. Sci. 21 (2004) 553–560.
[20] C.M. Waters, et al., Mechanobiology in lung epithelial cells: measurements, perturbations, and responses, Comp. Physiol. 2 (2012) 1–29.
[21] K.A. Foster, et al., Characterization of the A549 cell line as a type II pulmonary epithelial cell model for drug metabolism, Exp. Cell Res. 243 (1998) 359–366.
[22] S.T. Buckley, et al., Differential susceptibility to epithelial-mesenchymal transition (EMT) of alveolar, bronchial and intestinal epithelial cells in vitro and the effect of angiotensin II receptor inhibition, Cell Tissue Res. 342 (2010) 39–51.
[23] D. Huh, et al., Reconstituting organ-level lung functions on a chip, Science 328 (2010) 1662–1668.
[24] A.O. Stucki, et al., A lung-on-a-chip array with an integrated bio-inspired respiration mechanism, Lab Chip 15 (2015) 1302–1310.
[25] K.L. Sellgren, et al., A biomimetic multicellular model of the airways using primary human cells, Lab Chip 14 (2014) 3349–3358.
[26] C.E. Barkauskas, et al., Lung organoids: current uses and future promise, Development 144 (2017) 986–997.
[27] K. Gkatzis, et al., Use of three-dimensional organoids and lung-on-a-chip methods to study lung development, regeneration and disease, Eur. Respir. J. 52 (2018) 1800876.
[28] T. Liu, et al., Advanced micromachining of concave microwells for long term on-chip culture of multicellular tumor spheroids, ACS Appl. Mater. Interfaces 6 (2014) 8090–8097.
[29] M. Nikkhah, et al., Cytoskeletal role in differential adhesion patterns of normal fibroblasts and breast cancer cells inside silicon microenvironments, Biomed. Microdevices 11 (2009) 585–595.
[30] B. Wagner, et al., Microfabrication of complex surface topographies using grey-tone lithography, Sens. Actuators A Phys. 46 (1995) 89–94.
[31] J.Y. Park, et al., Study of cellular behaviors on concave and convex microstructures fabricated from elastic PDMS membranes, Lab Chip 9 (2009) 2043–2049.
[32] C.K.M. Ng, et al., Fabrication of substrates with curvature for cell cultivation by alpha-particle irradiation and chemical etching of PADC films, Nucl. Instrum. Methods Phys. Res. Sect. B Beam Interact. Mater. Atoms 278 (2012) 15–19.
[33] J.Y. Park, et al., Study of cellular behaviors on concave and convex microstructures fabricated from elastic PDMS membranes, Lab Chip 9 (2009) 2043–2049.
[34] A.K. Nguyen, R.J. Narayan, Two-photon polymerization for biological applications, Mater. Today 20 (2017) 314–322.
[35] M.I. Hermanns, et al., Lung epithelial cell lines in coculture with human pulmonary microvascular endothelial cells: development of an alveolo-capillary barrier in vitro, Lab. Invest. 84 (2004) 736–752.
[36] S.R. Polio, et al., Cross-platform mechanical characterization of lung tissue, PloS One 13 (2018), e0204765.
[37] T. Pasman, et al., Fabricating porous, photo-crosslinked poly(trimethylene carbonate) membranes using temperature-induced phase separation, Polym. Adv. Technol. 28 (2017) 1258–1262.
[38] M. Buitinga, et al., Micro-fabricated scaffolds lead to efficient remission of diabetes in mice, Biomaterials 135 (2017) 10–22.
[39] M. Buitinga, et al., Microwell scaffolds for the extrahepatic transplantation of islets of langerhans, PloS One 8 (2013) e64772.
[40] A.-K. Schneider, et al., DNA-SMART: biopatterned polymer film microchannels for selective immobilization of proteins and cells, Small 13 (2017) 1603923.
[41] J.P. Wikswo, et al., Scaling and systems biology for integrating multiple organs-on-a-chip, Lab Chip 13 (2013) 3496–3511.
[42] E.J. Vrij, et al., 3D high throughput screening and profiling of embryoid bodies in thermoformed microwell plates, Lab Chip 16 (2016) 734–742.
[43] M. Lieber, et al., A continuous tumor-cell line from a human lung carcinoma with properties of type II alveolar epithelial cells, Int. J. Canc. 17 (1976) 62–70.
[44] C.I. Grainger, et al., Culture of Calu-3 cells at the air interface provides a representative model of the airway epithelial barrier, Pharm. Res. (N. Y.) 23 (2006) 1482–1490.
[45] H.M. Creager, et al., In vitro exposure system for study of aerosolized influenza virus, Virology 500 (2017) 62–70.
[46] B.A. Hassell, et al., Human organ chip models recapitulate orthotopic lung cancer growth, therapeutic responses, and tumor dormancy in vitro, Cell Rep. 21 (2017) 508–516.
[47] L. Lin, et al., Krüpple-like-factor 4 attenuates lung fibrosis via inhibiting epithelial-mesenchymal transition, Sci. Rep. 7 (2017) 1–12.
[48] E. Cipolla, et al., IL-17A deficiency mitigates bleomycin-induced complement activation during lung fibrosis, FASEB J 31 (2017) 5543–5556.
[49] T. Yano, et al., KGF regulates pulmonary epithelial proliferation and surfactant protein gene expression in adult rat lung, Am. J. Physiol. Cell. Mol. Physiol. 279 (2000) L1146–L1158.
[50] B. Driscoll, et al., Isolation and characterization of distal lung progenitor cells, in: Methods in Mol. Biol., Humana Press, 2012, pp. 109–122.
[51] J.M. Liebler, et al., Combinations of differentiation markers distinguish subpopulations of alveolar epithelial cells in adult lung, Am. J. Physiol. Cell. Mol. Physiol. 310 (2015) L114–L120.
[52] K.A.A. Schilders, et al., Regeneration of the lung: lung stem cells and the development of lung mimicking devices, Respir. Res. 17 (2016) 44.
[53] P.F. Costa, et al., Mimicking arterial thrombosis in a 3D-printed microfluidic in vitro vascular model based on computed tomography angiography data, Lab Chip 17 (2017) 2785–2792.
[54] L.K. Fiddes, et al., A circular cross-section PDMS microfluidics system for replication of cardiovascular flow conditions, Biomaterials 31 (2010) 3459–3464.
[55] J.C.H. Poon, et al., Design of biomimetic substrates for long-term maintenance of alveolar epithelial cells, Biomater. Sci. 6 (2018) 292–303.
[56] W. Xi, et al., Emergent patterns of collective cell migration under tubular confinement, Nat. Commun. 8 (2017) 1517.
[57] T. Yamashita, et al., Cell sheet mechanics: how geometrical constraints induce the detachment of cell sheets from concave surfaces, Acta Biomater. 45 (2016) 85–97.
[58] N.J. Douville, et al., Combination of fluid and solid mechanical stresses contribute to cell death and detachment in a microfluidic alveolar model, Lab Chip 11 (2011) 609–619.
[59] L. Atia, et al., Geometric constraints during epithelial jamming, Nat. Phys. 14 (2018) 613–620.
[60] T.E. Angelini, et al., Glass-like dynamics of collective cell migration, Proc. Natl. Acad. Sci. U.S.A. 108 (2011) 4714–4719.
[61] M. Sadati, et al., Collective migration and cell jamming, Differentiation 86 (2013) 121–125.

[62] D. Bi, et al., Motility-driven glass and jamming transitions in biological tissues, Phys. Rev. X 6 (2016) 1–13.
[63] A. Haeger, et al., Cell jamming: collective invasion of mesenchymal tumor cells imposed by tissue confinement, Biochim. Biophys. Acta Gen. Subj. 1840 (2014) 2386–2395.
[64] S. Pawlizak, et al., Testing the differential adhesion hypothesis across the epithelial–mesenchymal transition, New J. Phys. 17 (2015), 083049.
[65] J.-A. Park, et al., Unjamming and cell shape in the asthmatic airway epithelium, Nat. Mater. 14 (2015) 1040–1048.
[66] M.C. Gibson, et al., The emergence of geometric order in proliferating metazoan epithelia, Nature 442 (2006) 1038–1041.
[67] M.E. Kreft, et al., The characterization of the human cell line Calu-3 under different culture conditions and its use as an optimized in vitro model to investigate bronchial epithelial function, Eur. J. Pharmaceut. Sci. 69 (2015) 1–9.
[68] H. Fehrenbach, Alveolar epithelial type II cell: defender of the alveolus revisited, Respir. Res. 2 (2001) 33–46.
[69] E.L. Herzog, et al., Knowns and unknowns of the alveolus, Proc. Am. Thorac. Soc. 5 (2008) 778–782.
[70] A.M. Kloxin, et al., Responsive culture platform to examine the influence of microenvironmental geometry on cell function in 3D, Integr. Biol. 4 (2012) 1540–1549.
[71] E.W. Gomez, et al., Tissue geometry patterns epithelial-mesenchymal transition via intercellular mechanotransduction, J. Cell. Biochem. 110 (2010) 44–51.